



## Multiway canonical correlation analysis of brain data

**de Cheveigné, Alain; Di Liberto, Giovanni M; Arzounian, Dorothée; Wong, Daniel D E; Hjortkjær, Jens; Fuglsang, Søren; Parra, Lucas C**

*Published in:*  
NeuroImage

*Link to article, DOI:*  
[10.1016/j.neuroimage.2018.11.026](https://doi.org/10.1016/j.neuroimage.2018.11.026)

*Publication date:*  
2018

*Document Version*  
Peer reviewed version

[Link back to DTU Orbit](#)

*Citation (APA):*  
de Cheveigné, A., Di Liberto, G. M., Arzounian, D., Wong, D. D. E., Hjortkjær, J., Fuglsang, S., & Parra, L. C. (2018). Multiway canonical correlation analysis of brain data. *NeuroImage*, 186, 728-740.  
<https://doi.org/10.1016/j.neuroimage.2018.11.026>

---

### General rights

Copyright and moral rights for the publications made accessible in the public portal are retained by the authors and/or other copyright owners and it is a condition of accessing publications that users recognise and abide by the legal requirements associated with these rights.

- Users may download and print one copy of any publication from the public portal for the purpose of private study or research.
- You may not further distribute the material or use it for any profit-making activity or commercial gain
- You may freely distribute the URL identifying the publication in the public portal

If you believe that this document breaches copyright please contact us providing details, and we will remove access to the work immediately and investigate your claim.

## **Multiway Canonical Correlation Analysis of Brain Signals**

Alain de Cheveigné(1, 2, 3), Giovanni M. Di Liberto (1, 2), Dorothée Arzounian (1,2), Daniel D.E. Wong (1,2), Jens Hjortkjær (4, 5), Søren Fuglsang (4), Lucas C. Parra (6)

### **AUTHOR AFFILIATIONS:**

- (1) Laboratoire des Systèmes Perceptifs, UMR 8248, CNRS, France
- (2) Département d'Etudes Cognitives, Ecole Normale Supérieure, PSL University, Paris, France
- (3) UCL Ear Institute, London, United Kingdom
- (4) Hearing Systems Group, Department of Electrical Engineering, Technical University of Denmark
- (5) Danish Research Centre for Magnetic Resonance, Centre for Functional and Diagnostic Imaging and Research, Copenhagen University Hospital Hvidovre
- (6) City College New York, USA

### **CORRESPONDING AUTHOR:**

Alain de Cheveigné, Audition, DEC, ENS, 29 rue d'Ulm, 75230, Paris, France,  
Alain.de.Cheveigne@ens.fr, phone 0033144322672, 00447912504027.

Keywords: EEG, MEG, LFP, ECoG, ICA, CSP, DSS, SNS, CCA, generalized CCA, multiple CCA, multiway CCA, multivariate CCA mcca gcca

# **Abstract**

Brain signals recorded with electroencephalography (EEG), magnetoencephalography (MEG) and related techniques often have poor signal-to-noise ratio due to the presence of multiple competing sources and artifacts. A common remedy is to average over repeats of the same stimulus, but this is not applicable for temporally extended stimuli that are presented only once (speech, music, movies, natural sound). An alternative is to average responses over multiple subjects that were presented with the same identical stimuli, but differences in geometry of brain sources and sensors reduce the effectiveness of this solution. Multiway canonical correlation analysis (MCCA) brings a solution to this problem by allowing data from multiple subjects to be fused in such a way as to extract components common to all. This paper reviews the method, offers application examples that illustrate its effectiveness, and outlines the caveats and risks entailed by the method.

## **1 Introduction**

Stimulus-driven signals recorded with electroencephalography (EEG), magnetoencephalography (MEG) and related techniques compete with much stronger sources within the brain, the body, and the environment. The signal of interest usually represents only a fraction of the signal power at the electrode or sensor. To overcome the noise and artifacts, a common practice is to present the same stimulus multiple times and average the responses over repeated presentations. Supposing that the response is the same for all presentations, and the noise is uncorrelated between presentations, the signal-to-noise power ratio (SNR) improves with the number of repeats. SNR can be further improved by combining signals across sensors, i.e. spatial filtering. Spatial filters can be optimized based on assumptions about signal and noise (de Cheveigné and Parra, 2014), and this

26 combination of temporal averaging and spatial filtering can greatly improve the  
27 SNR. However, averaging and optimization are not applicable if the stimulus is  
28 presented only once, for example because it is too long to be repeated (e.g. a long  
29 sample of speech or music), or because one wishes to probe a phenomenon likely  
30 to fade with repetitions (e.g. surprise).

31 Instead of presenting the same stimulus multiple times to one subject, one  
32 can also present the same stimulus to multiple subjects just once. To the extent  
33 that different subjects' brains are functionally similar, we expect similar responses  
34 (Hasson et al., 2004; Dmochowski et al., 2012; Lankinen et al., 2014). Unfortu-  
35 nately, the position or orientation of neural sources relative to sensors or electrodes  
36 is likely to differ across subjects, so averaging over subjects in sensor space is sub-  
37 optimal. In order to compare between subjects, or average over subjects, we first  
38 need some way to transform the data of each to a common representation that is  
39 comparable across subjects. This can be accomplished with spatial filters that are  
40 tuned to each individual subject (e.g. Haxby et al., 2011; Lankinen et al., 2014).

41 Canonical Correlation Analysis (CCA) is a powerful technique to find lin-  
42 ear components that are correlated between two data matrices (Hotelling, 1936).  
43 Given two matrices  $\mathbf{X}_1$  and  $\mathbf{X}_2$  of size  $T \times d_1$  and  $T \times d_2$ , CCA produces trans-  
44 form matrices  $\mathbf{V}_1$  and  $\mathbf{V}_2$  of sizes  $d_1 \times d_0$  and  $d_2 \times d_0$ , where  $d_0$  is at most equal  
45 to the smaller of  $d_1$  and  $d_2$ . The columns of  $\mathbf{Y}_1 = \mathbf{X}_1 \mathbf{V}_1$  are of norm 1 and mutu-  
46 ally uncorrelated between each other, as are the columns of  $\mathbf{Y}_2 = \mathbf{X}_2 \mathbf{V}_2$ , while,  
47 more importantly, corresponding columns from each ("canonical correlate pairs")  
48 are maximally correlated. The first pair of canonical correlates (CC) defines the  
49 linear combinations of each data matrix with the *highest possible correlation* be-  
50 tween them. The next pair of CCs defines the most highly correlated combination  
51 that is uncorrelated from the first pair, and so-on. Applied to data from two sub-  
52 jects, CCA can find spatial filters that maximize the brain activity common to

53 both, transforming both subject's data so that they can more easily be compared  
54 or averaged. However, CCA does not address the issue of comparing or merging  
55 responses across more than two subjects.

56 Extensions to connect multiple data matrices have been proposed under names  
57 such as *multiple CCA* (Gross and Tibshirani, 2015; Witten and Tibshirani, 2009),  
58 *multiway CCA* (Sturm, 2016; Zhang et al., 2011), *multiset CCA* (Takane et al.,  
59 2008; Correa et al., 2010b,a; Hwang et al., 2012; Lankinen et al., 2014; Zhang  
60 et al., 2017; Via, Javier, Ignacio Santamaria and Pérez, 2005; Li et al., 2009), or  
61 *generalized CCA* (Kiers et al., 1994; Afshin-Pour et al., 2012; Melzer et al., 2001;  
62 Tenenhaus, 2011; Tenenhaus et al., 2015; Velden, 2011; Fu et al., 2017). This  
63 diversity in names covers a diversity of formulations (Kettenring, 1971) that all  
64 share the aim of finding components that are similar across data matrices. Recent  
65 progress addresses regularization (Tenenhaus, 2011), sparsity (Fu et al., 2017;  
66 Tenenhaus et al., 2015), missing data (van de Velden and Takane, 2012), nonlin-  
67 earity (Melzer et al., 2001), or deep learning (Benton et al., 2017). Using similar  
68 techniques, independent Component Analysis (ICA) has been generalized under  
69 the name of group ICA (GICA) (Eichele et al., 2011; Calhoun and Adali, 2012;  
70 Huster et al., 2015; Huster and Raud, 2018).

71 CCA has been used extensively for brain data analysis and modality fusion  
72 (Sui et al., 2012; Dähne et al., 2015; Dmochowski et al., 2017), and several studies  
73 have applied multiway CCA (MCCA) and variants thereof to merge data across  
74 subjects (Correa et al., 2010b; Afshin-Pour et al., 2012, 2014; Lankinen et al.,  
75 2014; Zhang et al., 2017; Li et al., 2009; Hwang et al., 2012; Karhunen et al.,  
76 2013; Haxby et al., 2011; Lankinen et al., 2014; Sturm, 2016; Zhang et al., 2017;  
77 Lankinen et al., 2018). This paper builds on those studies with the aim to better  
78 understand the range of applicability of the tool, what is achieved, and what are  
79 the caveats. We describe a simple formulation of MCCA that is easy to understand

80 and explain.

81 We show that MCCA can be applied effectively to multi-subject datasets of  
82 EEG or fMRI, both to *denoise* the data prior to further analyses, and to *summarize*  
83 the data and reveal traits common across the population of subjects. MCCA-  
84 based denoising yields significantly better scores in an auditory stimulus-response  
85 classification task, and MCCA-based joint analysis of fMRI data reveals detailed  
86 subject-specific activation topographies. The aims of this paper are (a) to provide  
87 an intuitive understanding of MCCA, (b) investigate ways in which it can be put  
88 to use, and (c) demonstrate its effectiveness for a range of common tasks in the  
89 analysis of brain data.

## 90 2 Methods

91 In this section we describe a simple formulation of MCCA, show how it can be  
92 applied to a variety of tasks, and give details of the real and synthetic data sets  
93 used by the examples reported in the Results.

### 94 2.1 Data analysis

95 **Signal model.** Assume a data set consisting of  $N$  data matrices, each comprised  
96 of a time series matrix  $\mathbf{X}_n$  of dimensions  $T$  (time)  $\times$   $d_n$  (channels). These could  
97 represent EEG, MEG or fMRI data recorded from  $N$  different subjects in response  
98 to the same stimulus. They could also be data from multiple imaging modalities  
99 gathered from the same subject. Each matrix  $\mathbf{X}_n$  consists of linear combinations  
100 of a set of sources  $\mathbf{S}$  common to all data matrices, to which is added a “noise” ma-  
101 trix  $\mathbf{N}_n$  of sources uncorrelated with  $\mathbf{S}$ , and uncorrelated with the noise matrices  
102  $\mathbf{N}_{n' \neq n}$  added to the other data matrices:

$$\mathbf{X}_n = \mathbf{A}_n \mathbf{S} + \mathbf{N}_n, \quad (1)$$

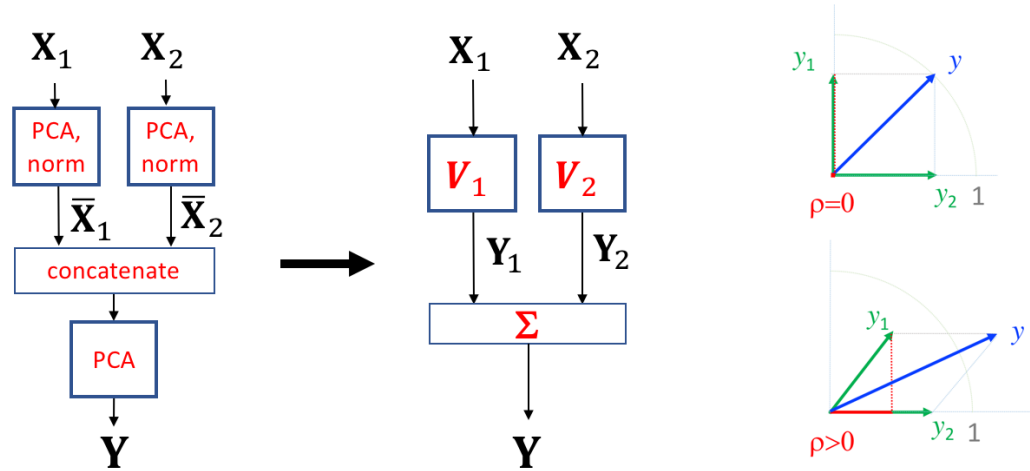


Figure 1: Block diagram of the simple CCA formulation. Left: each data matrix is whitened by PCA followed by normalization. Normalized PCs from both data matrices are concatenated side by side and submitted to a final PCA. Center: the matrix  $\mathbf{Y}$  of summary components (SC) can be expressed as the sum of individual transforms  $\mathbf{Y}_1 = \mathbf{X}_1 \mathbf{V}_1$  and  $\mathbf{Y}_2 = \mathbf{X}_2 \mathbf{V}_2$  (canonical correlates, CC). The transforms  $\mathbf{V}_1$  and  $\mathbf{V}_2$  combine the whitening and PCA matrices. Right: rotating vectors  $y_1$  and  $y_2$  to maximize the norm of their sum is equivalent to maximizing their correlation coefficient  $\rho$  symbolized by the projection of  $y_1$  on  $y_2$  (red line).

103 where  $\mathbf{A}_n$  is a mixing matrix specific to subject  $n$ . The sources  $\mathbf{S}$  might represent  
104 brain sources or networks driven by the same stimulus similarly across different  
105 subjects. We are interested in finding these “shared sources” and suppressing the  
106 noise. Note that this model assumes that responses of different subjects share  
107 the same source *time course*, but not necessarily the same spatial pattern over  
108 channels. The assumption of uncorrelated noise is usually only approximately  
109 met, due to spurious correlations.

110 **A simple CCA formulation.** Consider two data matrices,  $\mathbf{X}_1$  and  $\mathbf{X}_2$  of size  
111  $T \times d$  where  $T$  is time and  $d$  the number of channels. All data are assumed to have



112 zero mean. Each matrix is spatially whitened by applying principal component  
113 analysis (PCA) and scaling each principal component (PC) to unit norm to obtain  
114 whitened matrices  $\bar{\mathbf{X}}_1$  and  $\bar{\mathbf{X}}_2$ . Whitened data are then concatenated and submit-  
115 ted to a new PCA to obtain a matrix  $\mathbf{Y} = [\mathbf{X}_1, \mathbf{X}_2]\mathbf{V}$  of size  $T \times 2d$ , where  $\mathbf{V}$   
116 combines the whitening and second PCA matrices (Fig. 1 left). The submatrices  
117  $\mathbf{V}_1$  and  $\mathbf{V}_2$  formed of the first and last  $d$  rows of  $\mathbf{V}$  define transforms applicable  
118 to each data matrix:

$$\begin{aligned}\mathbf{Y}_1 &= \mathbf{X}_1 \mathbf{V}_1, \\ \mathbf{Y}_2 &= \mathbf{X}_2 \mathbf{V}_2,\end{aligned}\tag{2}$$

119 with  $\mathbf{Y} = \mathbf{Y}_1 + \mathbf{Y}_2$  (Fig. 1 center).

120 The outcome of this analysis is equivalent to standard CCA, as explained in  
121 the Discussion, the first  $d$  columns of  $\mathbf{Y}_1$  and  $\mathbf{Y}_2$  forming canonical pairs (within  
122 a scaling factor). Indeed, rotating  $\bar{\mathbf{X}}_1$  and  $\bar{\mathbf{X}}_2$  to maximize the correlation of the  
123 resulting  $\mathbf{Y}_1$  and  $\mathbf{Y}_2$ , as required by the CCA objective, is equivalent to rotating  
124 with the goal of maximizing the norm of their sum,  $\mathbf{Y}_1 + \mathbf{Y}_2$ , as achieved by  
125 the second PCA (Fig. 1 right). The appeal of this formulation is that it is easily  
126 extendable to multiple data matrices.

127 **A simple MCCA formulation.** Consider  $N$  data matrices  $\mathbf{X}_n$  each of size  $T \times d$   
128 with zero mean. Each data matrix is spatially whitened by applying PCA and  
129 scaling all PCs to unit norm to obtain whitened matrices  $\bar{\mathbf{X}}_n$ . Whitened data are  
130 then concatenated along the component dimension and submitted to a second PCA  
131 to obtain a matrix  $\mathbf{Y} = [\mathbf{X}_1 \dots \mathbf{X}_N]\mathbf{V}$  of size  $T \times D$ ,  $D = Nd$ , where  $\mathbf{V}$  combines  
132 the whitening and second PCA matrices (Fig. 2 left). The submatrices  $\mathbf{V}_n$  of  $\mathbf{V}$  of  
133 size  $d \times D$  formed by extracting successive  $d$ -row blocks of  $\mathbf{V}$  define transforms  
134 applicable to each data matrix:

$$\mathbf{Y}_n = \mathbf{X}_n \mathbf{V}_n,\tag{3}$$

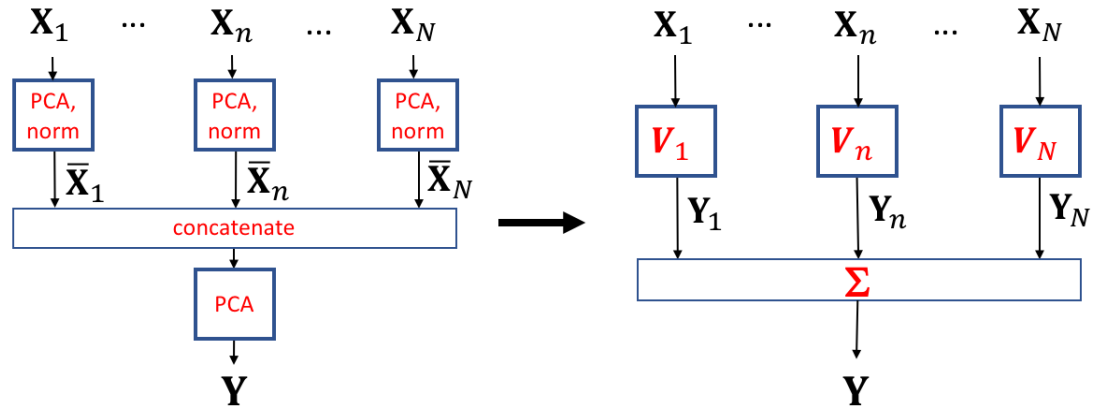


Figure 2: Block diagram of the simple MCCA formulation. Left: each data matrix  $\mathbf{X}_n$  is whitened by PCA followed by normalization. Normalized PCs from all data matrices are concatenated side by side and submitted to a final PCA. Right: the matrix  $\mathbf{Y}$  of summary components (SC) can be expressed as the sum of individual transforms  $\mathbf{Y}_n = \mathbf{X}_n \mathbf{V}_n$  (canonical correlates, CC).

135 with  $\mathbf{Y} = \sum_n \mathbf{Y}_n$  (Fig. 2, right). If data matrices have different numbers of chan-  
 136 nels  $d_n$ , then  $\mathbf{V}_n$  has size  $d_n \times D$  where  $D = \sum_n d_n$ . We call the columns of  $\mathbf{Y}_n$   
 137 *canonical correlates* (CCs) by analogy with CCA, and those of  $\mathbf{Y}$  *summary com-*  
 138 *ponents* (SC). Each SC is a sum of CCs over data sets. Columns of  $\mathbf{Y}$  are mutually  
 139 orthogonal by virtue of the final PCA, but the same is not usually true of  $\mathbf{Y}_n$ . With  
 140  $D > d$  columns,  $\mathbf{Y}_n$  forms an *overcomplete basis* of the patterns spanned by  $\mathbf{X}_n$ .  
 141 This formulation of MCCA is equivalent to the SUMCORR formulation of Ket-  
 142 tenring (1971) as explained in the Discussion (Parra, 2018). The appeal of this  
 143 formulation is that it is conceptually and computationally straightforward. PCs  
 144 can be discarded from the initial PCAs, so as to control dimensionality and limit  
 145 overfitting effects (next section).

146 The variances of the summary components (the columns of  $\mathbf{Y}$ ) reflect the de-  
 147 gree to which temporal patterns are shared between data matrices (Fig. 3) – the  
 148 variance of each SC corresponding to the degree of correlation of each shared

149 dimension found in the data. If the data matrices  $\mathbf{X}_n$  share no components, the  
 150 variances of all SCs are one (Fig. 3 a). If a component is shared by all  $N$  data  
 151 matrices, the norm of the first SC is  $N$  (Fig. 3 d). For data matrices with a small  
 152 number of samples, spurious correlations may cause the variance profile to be  
 153 skewed (Fig. 3 b). In real data, shared activity often shows up as components with  
 154 variance elevated relative to this background (Fig. 3 c).

155 **Reduced-rank MCCA.** It is often convenient to reduce the rank of each data  
 156 matrix  $\tilde{\mathbf{X}}_n$  to  $\mathring{d} < d$  by discarding PCs with smallest variance after the initial  
 157 PCA. The MCCA transform matrices  $\mathbf{V}_n$  are then of size  $d \times \mathring{D}$ ,  $\mathring{D} = N\mathring{d}$ , and  
 158 the CC and SC matrices of size  $T \times \mathring{D}$ . This serves as a form of regulariza-  
 159 tion that avoids computational issues with rank-deficient data, reduces the risk of  
 160 overfitting, and limits computation and memory requirements. Importantly, this  
 161 approach preserves the constraint that the resulting SCs are uncorrelated (Parra et  
 162 al., 2018).

163 **Dealing with data matrices with more channels than samples.** CCA fails if  
 164 the data matrices have fewer samples than channels ( $T \leq d$ ), as is typically the  
 165 case for fMRI or calcium imaging data for which there are many more voxels or  
 166 pixels than observation samples (Asendorf, 2015). A simple solution is to replace  
 167 each data matrix  $\mathbf{X}_n$  (size  $T \times d$ ) by a matrix  $\tilde{\mathbf{X}}_n$  of size  $T \times \mathring{T}$  with  $\mathring{T} < T$   
 168 columns that capture the principal temporal patterns spanned by  $\mathbf{X}_n$ . This can be  
 169 done by applying singular value decomposition (SVD) to express the data as

$$\mathbf{X}_n = \mathbf{U} \mathbf{S}^t \mathbf{V} \quad (4)$$

170 and setting  $\tilde{\mathbf{X}}_n = \mathring{\mathbf{U}}$  where  $\mathring{\mathbf{U}}$  consists of the first  $\mathring{T}$  columns of  $\mathbf{U}$ . Since the  $\tilde{\mathbf{X}}_n$   
 171 have more samples than channels there is no obstacle to applying MCCA to them.  
 172 This sequence of operations can be represented by a set of transform matrices

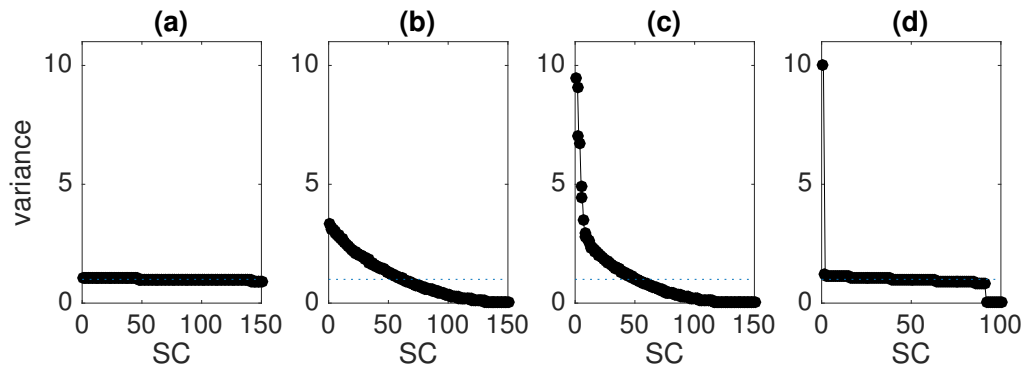


Figure 3: Behavior of the SC variance as a function of order for MCCA analyses applied to 4 different types of dataset, each involving 10 data matrices. (a) Each data matrix consisted of an independent  $10000 \times 15$  matrix of Gaussian white noise. In this case the SC variance profile is flat since there is no (or little) correlation between data matrices. (b) Each data matrix consisted of a  $165 \times 15$  matrix of independent and uncorrelated Gaussian noise. In this case the SC variance profile is skewed, reflecting spurious numerical correlations between the statistically independent columns. (c) Each data matrix consisted of a  $165 \times 15$  matrix of values derived from fMRI responses of 10 subjects in response to 165 sounds. Prior to MCCA the 6309 voxels were reduced to 15 channels using SVD (see description of Example 6 in the Methods). (d) Each data matrix consisted of a  $10000 \times 10$  matrix of Gaussian white noise with an embedded sinusoid (Example 1, Fig. 4) that was the same in all data matrices. In the last two examples, only a small subset of the MCCA components reflect shared activity as evident by the low SC variance at higher MCCA orders.

173  $\mathbf{V}_n$  of size  $d \times NT$ . Applying them to the data yields canonical correlate and  
 174 summary matrices of size  $T \times NT$ . Using this approach, it is straightforward to  
 175 apply MCCA to datasets with a large number of “channels” such as data from  
 176 calcium imaging or fMRI. An alternative to SVD is to apply PCA to  $\mathbf{X}_n$  and use  
 177 a subset of the matrix of projection vectors to form  $\tilde{\mathbf{X}}_n$ , a useful option if  $\mathbf{X}_n$  is  
 178 too large to fit in memory (the required covariance matrix can be calculated in  
 179 chunks).

## 180 2.2 Applications of MCCA

181 **Quantifying correlation between  $N$  data matrices.** The variance of each col-  
 182 umn of  $\mathbf{Y}$  indicates the degree to which a component is shared across data ma-  
 183 trices. The value is 1 if the data matrices are perfectly uncorrelated, and  $N$  if all  
 184 data matrices include that component (Fig. 3). The profile of variances over SCs  
 185 thus offers a measure of “sharedness” between data matrices (but see Caveats).

186 **Summarizing a set of data matrices.** The first few columns of  $\mathbf{Y} = \sum_n \mathbf{Y}_n$   
 187 represent temporal patterns that capture most of the correlation across data ma-  
 188 trices  $\mathbf{X}_n$ . They form a basis of the signal subspace that contains those shared  
 189 patterns.

190 **Denoising.** Each data matrix  $\mathbf{X}_n$  may be denoised by projecting it to the over-  
 191 complete basis of CCs, selecting the first  $\tilde{D} < D$  components, and projecting  
 192 back. We refer to this procedure as “denoising”, as it can be used to attenuate  
 193 components that are least shared across subjects. This can be summarized by a  
 194 denoising matrix  $\mathbf{D}_n$  product of the first  $\tilde{D}$  columns of  $\mathbf{V}_n$  by the first  $\tilde{D}$  rows of  
 195 its pseudoinverse. The denoised data are obtained as  $\tilde{\mathbf{X}}_n = \mathbf{X}_n \mathbf{D}_n$ .

196 **Dimensionality reduction.** Dimensionality reduction is often performed by ap-  
 197 plying PCA to a data matrix and truncating the PC series (Cunningham and Yu,  
 198 2014). However, this equates relevance to variance, which may not be appropriate  
 199 because noise sources can have high variance and useful targets small variance.  
 200 MCCA can be used to weight dimensions according to their *consistency across*  
 201 *data matrices*, which may be a better criterion than variance.

202 **Outlier detection.** Temporally-local glitches and artifacts may interfere with  
 203 data interpretation and analysis. Analysis algorithms based on least-squares are  
 204 particularly sensitive to high-amplitude artifacts. MCCA can be used to derive  
 205 a cross-subject ‘consensus’ response, so that individual subject’s data points that  
 206 deviate greatly from the consensus can be flagged as outliers and excluded from  
 207 analysis.

## 208 **2.3 Details of the evaluation examples**

209 The methods are evaluated using six datasets, including synthetic data, EEG, and  
 210 fMRI.

211 **Example 1 - sinusoidal target in separable noise.** Synthetic data for this ex-  
 212 ample consisted of 10 data matrices, each of dimensions 10000 samples  $\times$  10  
 213 channels. Each was obtained by multiplying 9 Gaussian noise signals (indep-  
 214 endent and uncorrelated) by a  $9 \times 10$  mixing matrix with random coefficients. To  
 215 this background of noise was added a “target” consisting of a sinusoidal time se-  
 216 ries (Fig. 4, left) multiplied by a  $1 \times 10$  mixing matrix with random coefficients.  
 217 The target was the same for all data matrices, but the mixing matrices differed, as  
 218 did the noise sources. The SNR was set to  $10^{-20}$ , i.e. a very unfavorable SNR,  
 219 but because the noise is not of full rank the target and background are in principle

220 linearly separable.

221 **Example 2 - sinusoidal target in non-separable noise.** Synthetic data for this  
 222 example consisted of 10 matrices of dimensions 10000 samples  $\times$  10 channels,  
 223 each obtained by multiplying 10 Gaussian noise sources (independent and uncor-  
 224 related) by a  $10 \times 10$  mixing matrix with random coefficients. To this background  
 225 was added a sinusoidal target as in the previous example, with SNR varied as a  
 226 parameter. The noise here is full rank so the target and background are not linearly  
 227 separable.

228 **Example 3 - sinusoidal target in EEG noise.** Data for this example used EEG  
 229 to simulate realistic neural activity as background noise. EEG data were recorded  
 230 during approximately 20 minutes from one subject in the absence of any task,  
 231 from 40 electrodes (32 standard positions plus additional electrodes on forehead  
 232 and temple) at 2048 Hz sampling rate with a BioSemi system. A robust polyno-  
 233 mial detrending routine (de Cheveigné and Arzounian, 2018) was used to remove  
 234 slow drifts. Ten “data matrices” were produced by selecting three-second inter-  
 235 vals of EEG data with random offsets, removing their means, and adding a target  
 236 consisting of 4 cycles of a 4 Hz sinusoid multiplied by a  $1 \times 40$  mixing matrix  
 237 with random coefficients, renewed for each data matrix. The SNR of the target  
 238 was varied as a parameter.

239 **Example 4 - EEG response to tones.** Data for this example were borrowed  
 240 from a study on auditory attention (Southwell et al., 2017). EEG data were  
 241 recorded using a 64-channel EEG system in response to 120 repetitions of a 1  
 242 kHz tone pip with interstimulus interval (ISI) randomized between 750 and 1550  
 243 ms (recorded for the purpose of locating electrodes responsive to sound). Data  
 244 from a subset of 10 subjects were detrended using a robust detrending routine,

bad channels were interpolated using spherical interpolation (EEGLAB), and the data were filtered between 2-45 Hz. A peristimulus epoch of duration 1.2 s (starting 0.2 s prestimulus) was defined for each trial, and the corresponding data were extracted as a 3D matrix of dimensions time  $\times$  channel  $\times$  trial. For each channel, the 0.2 s prestimulus waveform was averaged over trials and subtracted from that channel's waveform ("baseline correction"). After applying the first PCA (of the two-step MCCA) to each subject, the first 30 PCs were retained and the remainder discarded.

Two analyses were performed on these data to try to extract the cortical response to the 1 kHz tone from the background EEG noise. In the first, repetition over trials was exploited to design a spatial filter for each subject using the joint diagonalization algorithm (JD) that maximizes the ratio of trial-averaged variance to total variance (de Cheveigné and Simon, 2008; de Cheveigné and Parra, 2014). This resulted in a set of 10 analysis matrices of size  $64 \times 30$ , one for each subject. In the second analysis, MCCA was applied, using 30 PCs from each subject in the first PCA, resulting in 10 subject-specific analysis matrices of size  $64 \times 300$ .

For each subject, the first column of the JD analysis matrix defines the best linear combination of channels to maximize repeat-reliability across trials, while the first column of the MCCA analysis matrix defines the best linear combination of channels to maximize correlation with the other subjects.

**Example 5 - EEG response to speech.** Data for this example were taken from a study on auditory cortical responses to natural speech (Di Liberto et al., 2015). The same data were also used in a recent study on the application of CCA to speech/EEG decoding (de Cheveigné et al., 2018). We borrowed the data from the first study, and the decoding methods and evaluation metrics from the second, with the purpose of evaluating the benefit of introducing a denoising stage based



271 on MCCA before the speech/EEG decoding stage.

272 In brief, EEG data were recorded from 8 subjects using a 128-channel BioSemi  
273 system with standard electrode layout, at 512 Hz sampling rate. Each subject lis-  
274 tened to 32 speech excerpts, each of duration 155 s, from an audio book, presented  
275 diotically via headphones, for a total of approximately 1.4 hours. The database in-  
276 cluded both the audio stimuli and the EEG responses. Further details about the  
277 stimulus and recording are available in Di Liberto et al. (2015). The EEG were  
278 preprocessed (downsampling to 64 Hz, detrending, artifact removal), and the stim-  
279 ulus temporal envelope calculated as described in de Cheveigné et al. (2018).

280 A decoding model (de Cheveigné et al., 2018; Dmochowski et al., 2017) was  
281 evaluated according to several metrics: correlation, d-prime, and percent-correct  
282 classification scores for a match vs mismatch classification task. The classification  
283 task consisted in deciding whether a segment of EEG matched the segment of  
284 stimulus of same duration that produced it (match) or some unrelated segment  
285 (mismatch). The duration of the segment was varied as a parameter from 1 to 64  
286 s.

287 This task is related to that of determining which of two concurrent voices is  
288 the focus of a listener’s attention (cocktail party phenomenon) (Ding and Simon,  
289 2012; Fuglsang et al., 2017; Lalor et al., 2009; Khalighinejad et al., 2017; Koski-  
290 nen and Seppä, 2014; Martin et al., 2014; Mesgarani and Chang, 2012; Mirkovic  
291 et al., 2015; O’Sullivan et al., 2014; Tiitinen et al., 2012; Zion Golumbic et al.,  
292 2013), of potential use for the “cognitive control” of an external device such as  
293 a hearing aid. The decoding model used CCA to relate the stimulus to the EEG  
294 response, producing multiple stimulus-response CC pairs that were used for dis-  
295 crimination. Further details of the decoding model, classification task, and metrics  
296 can be found in de Cheveigné et al. (2018). Here, we are only interested in know-  
297 ing if scores for single-source decoding are improved by introducing a stage of

298 EEG denoising based on MCCA.

299 For this denoising, the EEG data of each subject were submitted to MCCA,  
300 keeping 40 PCs in the first PCA, resulting in a  $128 \times 320$  analysis matrix for each  
301 subject. The first 110 columns of this matrix were multiplied by the first 110 rows  
302 of its pseudoinverse to yield a  $128 \times 128$  subject-specific denoising matrix. This  
303 has the effect of attenuating activity that is *least* correlated with the other subjects.

304 **Example 6 - fMRI response to natural sounds.** Data for this example were  
305 taken from a study that measured fMRI responses to natural sounds (Norman-  
306 Haignere et al., 2015). Responses were gathered from 10 subjects to each of 165  
307 sounds belonging to 11 categories including speech, music, animal vocalizations,  
308 and others. For each subject, the recording session was repeated either twice or  
309 3 times. See Norman-Haignere et al. (2015) for further details. For the present  
310 analysis, data for each subject were averaged over repeats and organized as a  
311 matrix  $\mathbf{X}_n$  of  $165 \text{ sounds} \times 6309 \text{ voxels}$  (voxels from both hemispheres were  
312 used, and voxels outside a subject-specific region of interest that included primary  
313 and secondary auditory cortex were set to zero). In this analysis we are interested  
314 in finding particular profiles of response over sounds (for example speech vs non-  
315 speech, or music vs non-music) and also the brain areas associated with such  
316 profiles in each subject.

317 As there are more "channels" (voxels) than samples ( $T < d$ ), an SVD was used  
318 as described in the Methods and the first 10 dimensions were used for MCCA. The  
319 columns of  $\overset{\circ}{\mathbf{X}}_n$  are white so the first PCA can be dispensed of. Matrices  $\overset{\circ}{\mathbf{X}}_n$  were  
320 concatenated and subjected to the second-step PCA of the MCCA algorithm, and  
321 the 15 first columns (arbitrary number) of the SC matrix were selected as a basis  
322 spanning the profiles over sounds that were most similar across subjects.

323 To find profiles specific to particular sound categories (e.g. speech, music,

etc.), Joint Decorrelation (de Cheveigné and Parra, 2014) was used to find a linear transform applicable to the 15-column basis to maximize the variance over the selected category, relative to the other categories. This can be seen as a rotation of the basis so as to isolate activity specific to processing of that sound category. This  $165 \times 1$  activation profile was then cross-correlated with the  $165 \times 6309$  matrix of fMRI response data of each subject to find the topography specific to that subject (Haufe et al., 2014).

## 3 Results

The MCCA method is evaluated first with synthetic data to get an understanding of its basic properties and capabilities, and then with real EEG and MEG data to see whether these extend to situations of practical use.

### 3.1 Synthetic data

**Example 1 - sinusoidal target in separable noise.** The data consist of 10 matrices made up of a sinusoidal target (Fig. 4, left) common to all data matrices, with added noise distinct across matrices (see Methods). At the unfavorable SNR of  $10^{-20}$  the target is not visible in the raw signal of any of the data matrices (Fig. 4 center), and it cannot be extracted by averaging because of the extremely low SNR and the fact that the mixing coefficients are of random sign. Since the data are separable (the rank of the noise is only 9), the target *can* be recovered by applying the appropriate demixing matrix (inverse of the mixing matrix), however that matrix is unknown.

MCCA applied to the dataset produced projection matrices  $\mathbf{V}_n$  that recover the target from  $\mathbf{X}_n$  (Fig. 4 right). This benefit is similar to that of methods that leverage multiple repetitions to blindly discover spatial filters to improve SNR

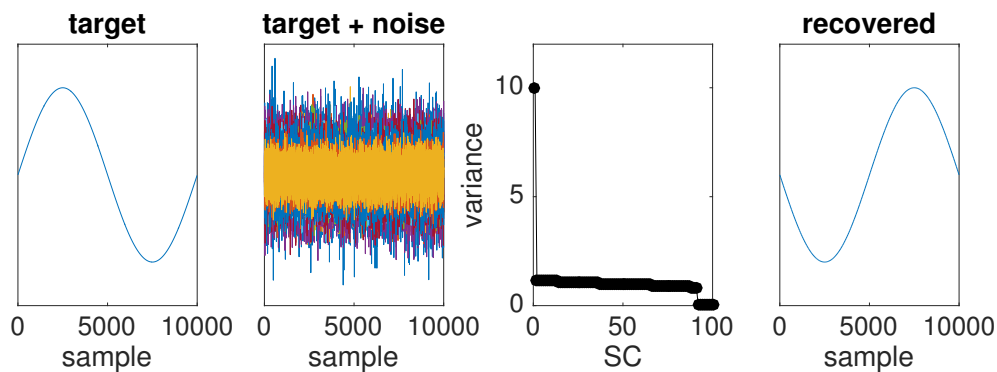


Figure 4: Simulation with separable noise. Left: target signal. Next to left: target in noise at  $\text{SNR}=10^{-20}$ . Next to right: variance of SCs as a function of order. The variance of the first SC is equal to 10 as target is perfectly shared across subjects and mixed in separable noise. Right: target recovered by MCCA (with arbitrary sign).

(de Cheveigné and Simon, 2008; de Cheveigné and Parra, 2014), but instead of repetitions, MCCA leverages the fact that the same target is mixed into multiple data matrices. To summarize, MCCA can reveal a target common across data matrices despite an extremely unfavorable SNR.

**Example 2 - sinusoidal target in non-separable noise.** Data are the same as in the previous example, except that the noise is full rank (10 independent sources mixed in 10 channels) so the target is no longer linearly separable, and one cannot expect to recover the target perfectly, especially at extremely low SNRs. Nonetheless, at a moderately unfavorable SNR ( $10^{-2}$  in power) MCCA can recover an estimate of the target that is noisy (Fig. 5 center) but much cleaner than the raw data (not shown). Figure 5 (right) shows the proportion of residual noise in the signal recovered by MCCA as a function of SNR, together with the same proportion for the best raw channel. MCCA provides a clear benefit over a range of SNRs. Two factors can contribute to failure: non-separability per se, and the fact that the algorithm fails to find the ideal demixing matrix. Figure 5 (right) also

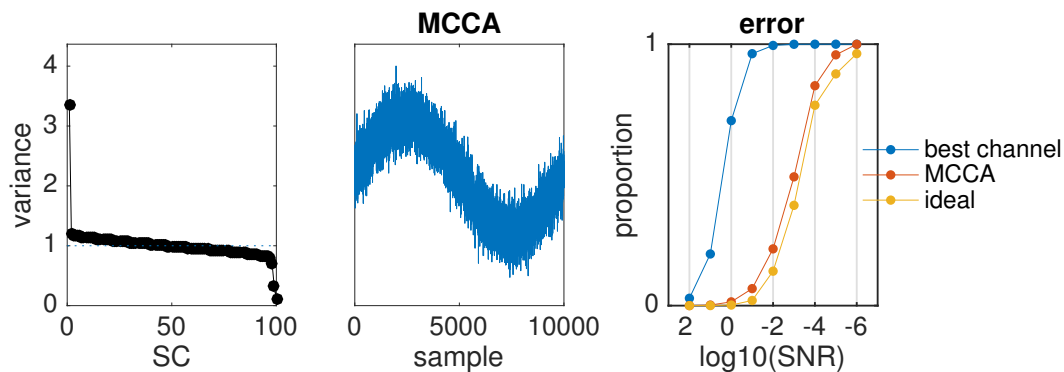


Figure 5: Simulation with inseparable noise. Left: variance of SCs as a function of their order at SNR=10<sup>-2</sup>. Center: target signal recovered from mixture at SNR=10<sup>-2</sup>. Right: proportion of residual noise power as a function of SNR for the raw data (blue), first SC (red) or ideal demixing matrix (yellow).

363 shows the proportion of residual noise for the ideal demixing matrix (yellow). The  
 364 MCCA-derived matrix performs only slightly less well than the ideal matrix. To  
 365 summarize, MCCA is of use even if the data are not separable.

366 **Example 3 - sinusoidal target in real EEG noise.** EEG background noise dif-  
 367 fers from the white Gaussian noise that was used in the previous simulations in  
 368 several ways: it usually has full rank (in particular because of electrode-specific  
 369 noise), but the variance is unequally distributed across dimensions. It is also  
 370 temporally structured, with strong temporal correlation and an overall low-pass  
 371 spectrum. The first component recovered by MCCA is plotted in Fig. 6 (right)  
 372 for several values of SNR. For SNRs of 0.1 or better the target is almost per-  
 373 fectly recovered. At SNR=0.03 the recovered waveform is somewhat noisy, and  
 374 at SNR=0.01 or below the target is lost. For comparison Fig. 6 (left) shows the  
 375 time course of a raw data channel (the channel that showed the largest correlation  
 376 with the target). For SNR=10 the target waveform is obvious in the raw data, but  
 377 for smaller values of SNR it is lost in the EEG noise. Comparing Fig. 6 left and

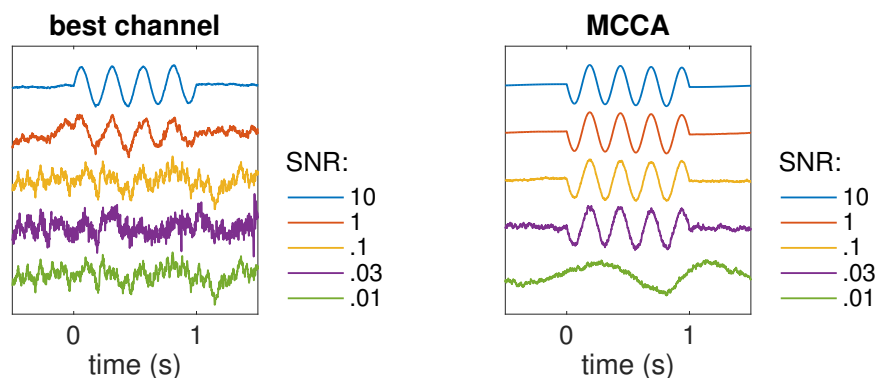


Figure 6: Simulation with EEG noise. Left: time course of the best raw data channel for several values of SNR. Right: time course of the first MCCA component for several values of SNR.

right, there is a range of SNRs (roughly 0.03 to 1) for which MCCA provides a clear benefit. Below SNR=0.03 the algorithm switched to some other component within the data (Fig. 6 right, lowest trace) that happened to be similar across data matrices because of random correlations.

To summarize, MCCA is effective at extracting a weak target from within real EEG noise.

### 3.2 Real data.

**Example 4 - EEG response to tones.** In this example, contrary to the previous one, the target is not known. However, since the data were collected in response to multiple repeats *and* for multiple subjects, we can apply two different methods (JD and MCCA) to isolate stimulus-evoked activity common to all subjects and compare the results. JD finds a linear transform that optimizes signal to noise ratio assuming that the signal repeats over trials. Figure 7 (top) shows the result of applying the JD analysis to the data of one subject. In the plot on the top left, the blue line shows the mean over repeats of the first component, and the gray band shows  $\pm 2$  SD of a bootstrap resampling of this mean. On the top right is

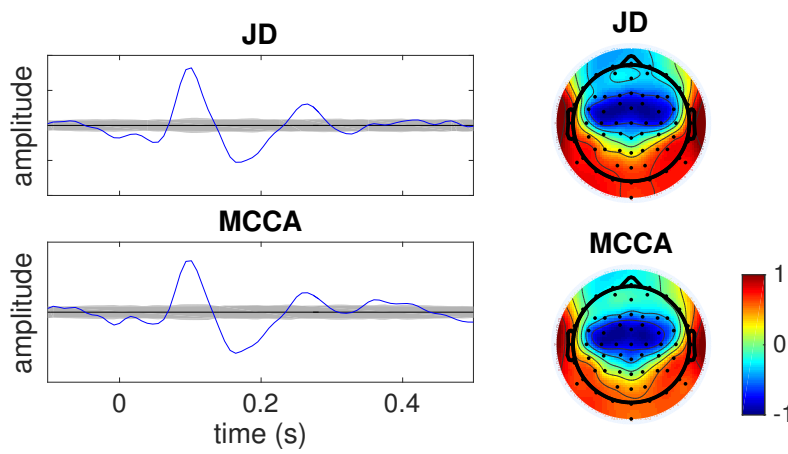


Figure 7: Comparison between JD solution (within-subject repeat-reliability) and MCCA solution (between-subject similarity) for one subject among ten. Data were in response to repeated tones. Left: average over trials (blue) and  $\pm 2$  SD of a bootstrap resampling (gray) of the first JD component, which maximizes reliability across trials (top), or first subject-specific CC (bottom). Right: associated topographies (correlation between trial-averaged component and trial-averaged electrode waveforms).

the topography associated with this component (computed as the map of cross-correlation coefficients between the component and each channel (Haufe et al., 2014)). MCCA can similarly be used to design a subject-specific spatial filter that improves SNR. The plots on the bottom of Figure 7 show the result of applying the subject-specific matrix derived from the MCCA analysis for the same subject. Despite the different criteria used by the two analyses (consistency over trials for JD, consistency between subjects for MCCA) the patterns are remarkably similar. To summarize, it appears that MCCA can exploit between-subject consistency to find a spatial filter that is as effective as that found by JD that exploits between-trial consistency. This is useful for data that do not involve repeated trials.

The subject-specific MCCA analysis matrices ( $V_n$ ) transform each subject's data ( $X_n$ ) into CCs ( $Y_n$ ) that are well correlated across subjects so that it makes

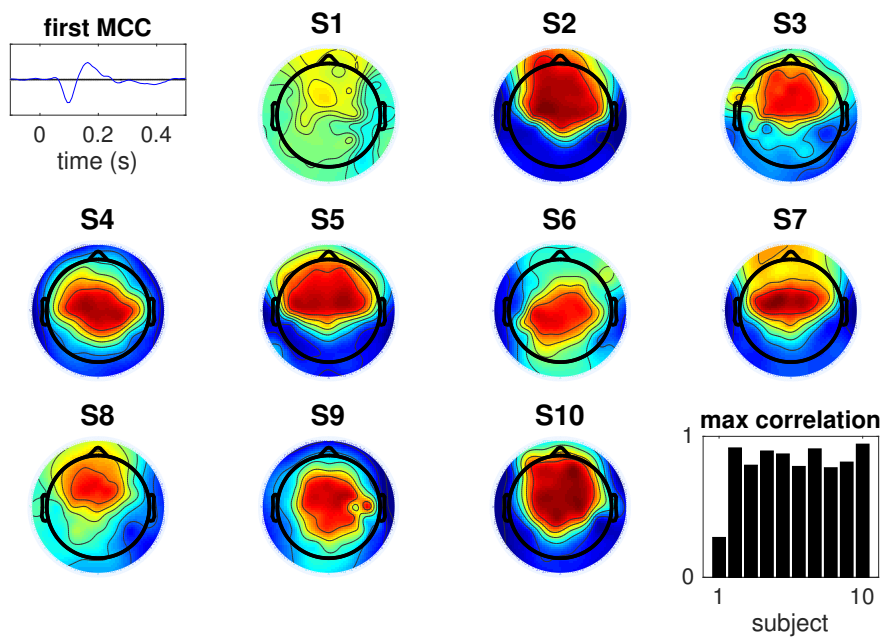


Figure 8: MCCA analysis of tone response, summary over 10 subjects. Top left: trial-averaged time course of the first SC. Bottom right: maximum absolute value of correlation between that component and each electrode, for each subject. Other panels: topography of correlation values (of the SC with each electrode) for each subject (the color code is the same as in Fig. 7, bottom).

406 sense to average them across subjects and interpret the SCs (Y) as reflecting  
 407 shared activity. Figure 8 top left shows the trial- and subject-averaged time course  
 408 of the first SC, which can be interpreted as our best estimate of stimulus-evoked  
 409 activity common to all subjects. It benefits from several stages of enhancement:  
 410 (a) spatial filtering within each subject, (b) averaging over trials, (c) averaging  
 411 across subjects. Also shown in Fig. 8 are the ten subject-specific topographies  
 412 associated with this component. Despite some differences, topographies are quite  
 413 similar across most subjects except S1. The bottom left plot shows the maxi-  
 414 mum over electrodes of the correlation coefficient between the first SC and each  
 415 electrode (trial-averaged). Correlation coefficients are relatively high except for  
 416 Subject 1 for whom the EEG response did not match the other subjects.



417 **Example 5 - EEG response to speech.** For stimuli presented once only, one  
 418 cannot use repetition to distinguish the brain response from the noise. Instead,  
 419 systems identification techniques (Lalor et al., 2009; Holdgraf et al., 2017; Crosse  
 420 et al., 2016) are used to fit an encoding model to estimate the part of brain response  
 421 that is driven by the stimulus, using some representation of the stimulus (e.g.  
 422 envelope or spectrogram) that can be linearly related to the brain signals. The part  
 423 of the response that fits the model can be taken as the “true” response, and the  
 424 rest discarded as noise. However, this partition is contingent on the validity of  
 425 the stimulus representation and the quality of the model. With MCCA, a “ground  
 426 truth” response can instead be estimated based on similarity of brain responses  
 427 across subjects.

428 EEG were recorded in response to continuous speech (see Methods), and a  
 429 model was fit to stimulus and response to capture their correlation (de Cheveigné  
 430 et al., 2018; Dmochowski et al., 2017). The model used CCA to form pairs of  
 431 maximally-correlated linear transforms of the audio stimulus features and of the  
 432 EEG respectively (audio-EEG CCs). Note that this usage of CCA is unrelated  
 433 to our usage of MCCA to merge data across subjects. The quality of that model  
 434 was evaluated using a match vs mismatch classification task (see Methods). We  
 435 compute *correlation*, *d-prime* and *percent correct* classification scores to evaluate  
 436 the benefit of inserting a stage of MCCA-based denoising within the EEG prepro-  
 437 cessing pipeline.

438 Figure 9 (a) shows the correlation between the first audio-EEG CC pair (thick  
 439 blue line) and subsequent pairs (thin lines), with and without MCCA-based de-  
 440 noising, for one subject. To the extent that correlation is limited in part by EEG  
 441 noise, the higher scores on the right suggest that denoising was effective. The  
 442 d-prime metric measures the degree of separation between distributions of cor-  
 443 relation scores for matched and mismatched segments. Figure 9 (b) shows the

d-prime metric for the first pair (thick blue) and subsequent pairs (thin lines), with and without MCCA-based denoising for segments of duration 64 s. The dotted line shows the d-prime metric for the multivariate distributions of audio-EEG CC pairs. The larger d-prime scores with MCCA-based denoising suggest that it can effectively contribute to improved discrimination. Figure 9 (c) shows classification scores as a function of segment duration with (red) and without (black) MCCA-based denoising. The higher scores with MCCA-based denoising show its benefit for this task. Figure 9 (d) shows that a similar benefit is found in all subjects. The thick lines are scores for a duration of 16 s, whereas the thin lines are for segments of 2 s (lowest lines) or 64 s (highest lines). To summarize, MCCA is of benefit as a denoising tool for EEG responses to speech.

**Example 6 - fMRI responses to natural sounds** Data were taken from a study that investigated fMRI responses to natural sounds (Norman-Haignere et al., 2015), in which 10 subjects listened to a set of 165 sounds belonging to 11 different classes. MCCA was applied to find patterns of selectivity to sound that were common across subjects as explained in the Methods. In brief, the  $165 \times 6309$  matrix of voxel activations for each subject was reduced to a  $165 \times 12$  matrix using SVD, the reduced matrices concatenated, and submitted to PCA to obtain a  $165 \times 120$  matrix of SCs. Their variances are plotted in Fig. 10 (top left). The first 10 SCs were subjected to a JD analysis to enhance the contrast between musical sounds (classes 'Music' + 'VocalMusic') and other sounds as explained in the Methods.

The profile of activation over sounds of the first JD component is plotted in Fig. 10 (top right), with sounds ordered by class and coded as different colors. Activations of the first two classes ('Music' + 'VocalMusic') are clearly distinct from that of the other classes. The corresponding topography of activation over voxels for each subject can be calculated by cross-correlating this component with

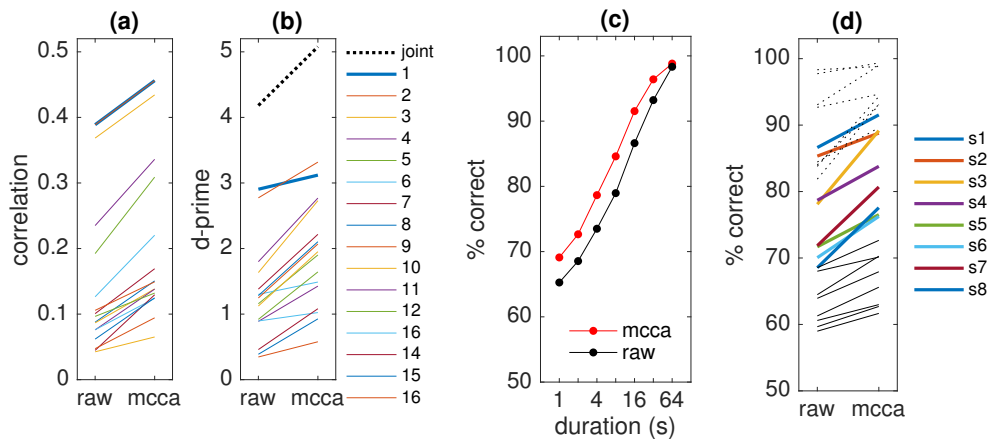


**Figure 9: Speech-EEG decoding.** (a) Correlation coefficient for the audio-EEG first CC pair (thick blue line) and subsequent pairs (thin lines) for a CCA model, with and without MCCA-based denoising. (b) d-prime metric for a classification task for the first audio-EEG CC pair (thick blue line) and subsequent pairs (thin lines), with and without MCCA-based denoising. The dotted line is for multivariate classification based on all CC pairs. (c) Percentage correct classification as a function of interval duration, with and without MCCA-based denoising. (d) Percentage correct for intervals of duration of 16s (thick lines) for 8 subjects, with and without MCCA-based denoising. Thin lines are scores for 64 s (uppermost) or 2 s (lowermost).

the profile of activation over sounds of each voxel. Topographies for the left hemisphere for all subjects are plotted in Fig. 10 (bottom). To a first approximation, topographies are consistent in that a dorso-frontal concentration of activity is found in most subjects. To a second approximation, each topography includes additional regions, suggesting a wider network of activation that is more subject-specific. Such subject-specific details would be smoothed out by averaging over subjects. A similar JD analysis to enhance speech-specific activation revealed patterns with more ventral topographies (not shown). The outcome of this analysis is consistent with that reported by Norman-Haignere et al. (2015) using an ICA-related technique.

The benefit of MCCA here can be interpreted in terms of dimensionality reduction, based here on *consistency across subjects* rather than variance as with PCA. Dimensionality reduction allowed the final JD analysis to be performed on a matrix of size  $165 \times 12 \times 10$  rather than  $165 \times 6309 \times 10$ , making it more effective by reducing overfitting. If PCA had been used instead of MCCA, the 12 selected dimensions might well have been dominated by noise. Using MCCA ensures that they are instead dominated by activity similar across subjects, which is likely to be relevant because all subjects heard the same stimuli.

This example demonstrates that MCCA can be applied also to data with more channels (pixels or voxels) than data points. MCCA offers a powerful, alternative, way of summarizing the high-dimensional data without having to explicitly model what parts of the brain response are driven by the stimulus features.

## 4 Discussion

MCCA finds a linear transform applicable to each data matrix within a data set to align them to common coordinates and reveal shared patterns. It can be used

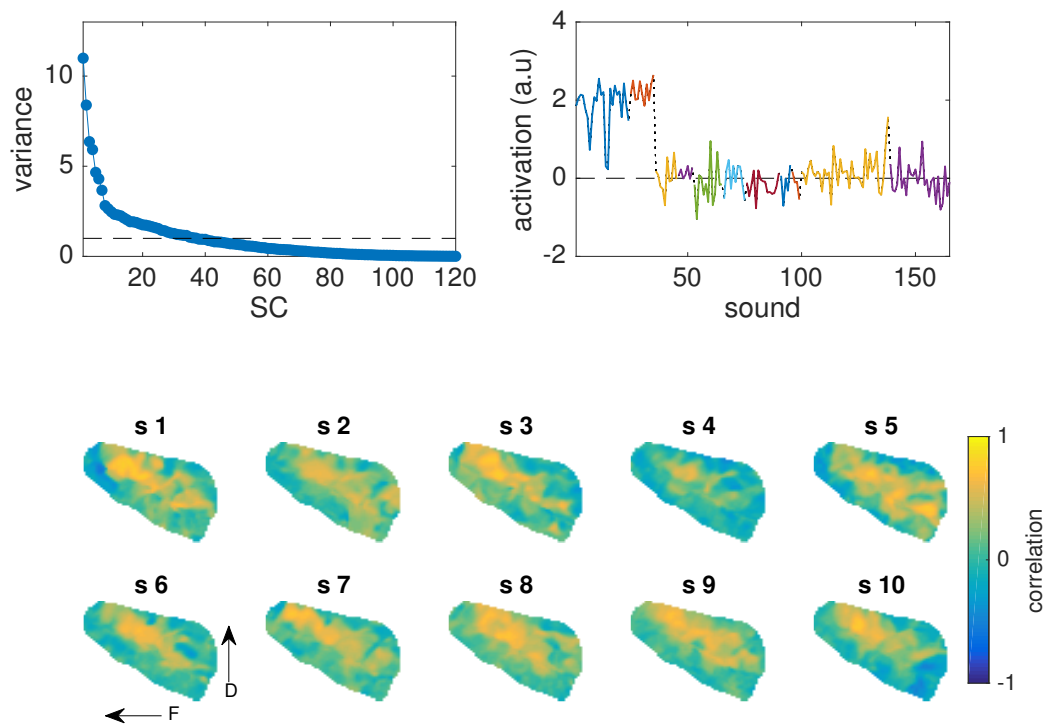


Figure 10: MCCA of fMRI responses to natural sounds. Top left: SC variance as a function of order. Top right: activation as a function of sound of a component selective for music obtained by applying JD to the first 15 SCs (see text). Each color represents a different sound category; the first two categories are 'music' and 'vocal music'. Bottom: topographies of correlation between the music-selective JD component and the profile of response over sound of each voxel of the right hemisphere, for each subject.

in several ways: as a *denoising* tool applicable to an individual data matrix, as a tool for *dimensionality reduction*, as a tool to *align* data matrices within a common space to allow comparisons, or as a tool to *summarize* data and reveal patterns that are general across data matrices. As formulated here, MCCA is easy to understand, straightforward to apply, and computationally cheap. Care is nonetheless required when applying it, in particular to avoid phenomena such as overfitting.

**What is new?** As reviewed in the Introduction, several versions of MCCA have been proposed in the literature and applied to the analysis of brain data. The contributions of this paper are the following. First, the formulation as a cascade of PCA, normalization, concatenation, and PCA offers an intuitive explanation that may help practitioners gain insight into this method. Past formulations may be hard to follow for the non-mathematically inclined, and their sheer number is bewildering. We used a similar 2-step formulation in a recent tutorial on joint decorrelation (de Cheveigné and Parra, 2014), and we hope that the present paper too will have tutorial value. Second, our usage of MCCA as a denoising tool, to attenuate noise within individual subjects based on across-subject consistency by projection on the overcomplete basis of its SCs, seems to be new. Third, we provide tutorial examples that may encourage researchers to put MCCA to work for a wider range of tasks, including denoising, outlier detection, summarization, and cross-subject statistics.

**How does it work?** The effect of the processing steps is schematized in Fig. 11. Multiple data matrices contain the same source component  $S$ , illustrated as a color gradient, mixed here into two 2-dimensional data matrices (Fig. 11 a). Each point represents a sample in time (row of the data matrix) and the two axes represent two channels (columns of the data matrix). The color could represent a hidden sensory response that is similar across two subjects. The initial PCAs sphere each

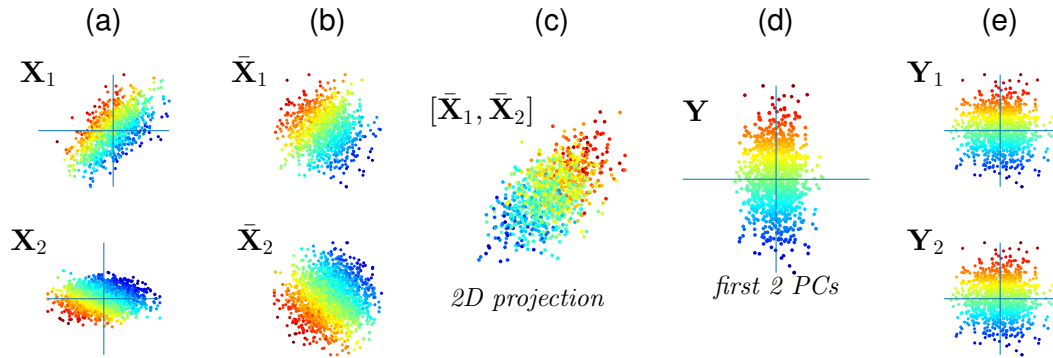


Figure 11: Principle of MCCA. (a) Several data matrices share a common component (coded as color) but its orientation and nature are unknown. (b) Whitening makes the data matrices free to rotate. (c) Concatenation creates a cloud in 4D space (projected here to 2D) with a direction of greater correlation/variance due to the shared component. (d) The second PCA aligns this direction with the axes. (e) In the process, the whitened data matrices are rotated such that shared dimensions are maximally aligned.

521 data matrix (b), so that the cloud of points is free to rotate in any direction. How-  
 522 ever, concatenating the sphered data matrices creates a cloud (in a 4-dimensional  
 523 space) that is not spherical because of the shared component correlation along  
 524 some direction in 4-D space (projected to 2D in panel (c)). The second PCA finds  
 525 this direction of correlation between the data matrices and aligns it with the first  
 526 axis (d), in the process transforming each data matrix so that it is optimally aligned  
 527 with the other (e).

528 **Relation with other formulations of CCA and MCCA** As explained by Parra  
 529 (2018), the aim of MCCA is to find projection vectors  $\mathbf{v}_n$  applicable to  $\mathbf{X}_n$  that  
 530 maximize the ratio of between-set to within-set covariance:

$$\rho = \frac{1}{N-1} \frac{r_B}{r_W} \quad (5)$$

531 with:

$$\begin{aligned} r_B &= \sum_n \sum_{n' \neq n} \mathbf{v}_n^T \mathbf{R}_{nn'} \mathbf{v}_{n'} \\ r_W &= \sum_n \mathbf{v}_n^T \mathbf{R}_{nn} \mathbf{v}_n. \end{aligned}$$

532 where  $\mathbf{R}_{nn} = \mathbf{X}_n^T \mathbf{X}_n$  and  $\mathbf{R}_{nn'} = \mathbf{X}_n^T \mathbf{X}_{n'}$  are covariance and cross-covariance  
533 matrices of the data. The divisor  $1 - N$  ensures that  $\rho$  scales between 0 and 1.  
534 Setting to zero the derivative of  $\rho$  with respect to  $\mathbf{v}_n$ , the solution is obtained by  
535 solving the equation

$$\mathbf{R}\mathbf{v} = \mathbf{D}\mathbf{v}\lambda, \quad (6)$$

536 with

$$\mathbf{R} = \begin{bmatrix} \mathbf{R}_{11} & \mathbf{R}_{12} & \cdots & \mathbf{R}_{1N} \\ \mathbf{R}_{21} & \mathbf{R}_{22} & \cdots & \mathbf{R}_{2N} \\ \vdots & \vdots & \ddots & \vdots \\ \mathbf{R}_{N1} & \mathbf{R}_{N2} & \cdots & \mathbf{R}_{NN} \end{bmatrix}, \mathbf{D} = \begin{bmatrix} \mathbf{R}_{11} & 0 & \cdots & 0 \\ 0 & \mathbf{R}_{22} & \cdots & 0 \\ \vdots & \vdots & \ddots & \vdots \\ 0 & 0 & \cdots & \mathbf{R}_{NN} \end{bmatrix}, \quad (7)$$

537 where  $\lambda = \rho/(N - 1) + 1$ . Now, first decompose  $\mathbf{D} = \mathbf{U}\mathbf{\Lambda}\mathbf{U}^T$ . Because  $\mathbf{D}$  is  
538 the block-diagonal matrix of the covariances in each data set, this decomposition  
539 implies doing PCA on each data set separately, i.e whitening each data set. With  
540 this decomposition Eq. 6 can be rewritten as:

$$\begin{aligned} \mathbf{R}\mathbf{v} &= \mathbf{U}\mathbf{\Lambda}\mathbf{U}^T\mathbf{v}\lambda \\ \mathbf{\Lambda}^{-1/2} \mathbf{U}^T \mathbf{R} \mathbf{v} &= \mathbf{\Lambda}^{1/2} \mathbf{U}^T \mathbf{v} \lambda \\ [\mathbf{\Lambda}^{-1/2} \mathbf{U}^T \mathbf{R} \mathbf{U} \mathbf{\Lambda}^{-1/2}] [\mathbf{\Lambda}^{1/2} \mathbf{U}^T \mathbf{v}] &= [\mathbf{\Lambda}^{1/2} \mathbf{U}^T \mathbf{v}] \lambda \\ \tilde{\mathbf{R}} \tilde{\mathbf{v}} &= \tilde{\mathbf{v}} \lambda \end{aligned} \quad (8)$$

541 where  $\tilde{\mathbf{R}} = \mathbf{\Lambda}^{-1/2} \mathbf{U}^T \mathbf{R} \mathbf{U} \mathbf{\Lambda}^{-1/2}$  is the covariance of the whitened concatenated  
542 data. Equation 8 thus corresponds to performing PCA on the concatenated whitened



543 data. In summary, the two-step PCA describe in the Methods ('simple MCCA  
544 formulation') maximizes correlation between data sets. This corresponds to the  
545 standard SUMCORR formulation of MCCA described by Kettenring (1971) (see  
546 Parra, 2018). The relations between this and other MCCA formulations are de-  
547 scribed in (Asendorf, 2015).

548 **MCCA vs CCA** MCCA is understood as a generalization of CCA but some dif-  
549 ferences are worth noting. For CCA the focus is usually on the CCs  $\mathbf{Y}_n$  ( $n = 1, 2$ ),  
550 whereas for MCCA it may also be on the SCs  $\mathbf{Y}$ . For standard CCA the projec-  
551 tion matrices are restricted to  $d$  (or  $\min_n d_n$ ) columns for each data set, whereas  
552 for MCCA it may be useful to consider more than  $d$  columns (as in Example 5). If  
553 the objective were to capture sources common to *all* data matrices,  $d$  components  
554 would suffice, but to capture also sources shared by *several sources but not all*,  
555 more than  $d$  columns are required. For CCA the  $d$  columns of  $\mathbf{Y}_1$  are mutually  
556 uncorrelated as are those of  $\mathbf{Y}_2$ , whereas for MCCA the  $D$  columns of  $\mathbf{Y}_n$  are mu-  
557 tually correlated in general. Columns of their sum  $\mathbf{Y}$  are uncorrelated, however.

558 The large number ( $D > d$ ) and non-orthogonality of the columns of  $\mathbf{Y}_n$  might  
559 be disconcerting for the researcher familiar with CCA. The method may be modi-  
560 fied such that  $\mathbf{Y}_n$  is instead constituted of  $d$  orthogonal columns. For this, MCCA  
561 is applied as above, for each  $n$  the first column of  $\mathbf{Y}_n$  is projected out of  $\mathbf{X}_n$ ,  
562 and MCCA applied again. This deflationary procedure terminates after  $d$  steps  
563 because the dimensionality of each data matrix is then exhausted. Smaller ma-  
564 trices with orthogonal columns might be convenient in certain situations, but as  
565 pointed out they might not capture all shared sources. The procedure described in  
566 the Methods is better in this respect.

567 **Group analysis of multi-subject data.** Gathering data from multiple subjects  
568 in response to the same stimulus serves several purposes. First, to counteract

variability by increasing the number of observations, analogous to recording from repeated trials. Second, to make inferences at the population level via group-level statistical analysis. Third, to allow data-dependent analysis to improve SNR based on similarity between subjects, analogous to methods that improve SNR based on similarity between trials (de Cheveigné and Parra, 2014).

The conventional strategy of calculating a “grand average”, with corresponding channels or voxels of each subject being averaged together (Choi et al., 2013; Luck, 2005), is hampered by inter-subject differences in source-to-sensor mapping. The problem is mild for sources with broad topographies (as in Fig. 8), but for sources with more local spatial characteristics a mismatch between subjects may result in destructive summation. A similar problem affects measures of inter-subject correlation (ISC) applied directly to channels or voxels (Hasson et al., 2004), or to linear combinations that assume the same mixing vectors for all subjects (Dmochowski et al., 2012; Parra et al., 2018).

One simple expedient is to select, for each subject, a group of channels based on responses to a “localizer” stimulus or task, calculate a root mean square average waveform over these channels, and then average these over subjects (e.g. Chait et al. (2010)). However, this packs the multidimensional cortical activity into a single time course from which it may be hard to infer the richer dynamics of cortical activity. Another approach is to apply inverse modeling to map the activity to a source space common across subjects (Litvak and Friston, 2008). However, this requires accurate anatomical information for each subject and is subject to the validity of the reconstruction models (Mahjoory et al., 2017), as well as between-subject variability in source positions and orientations (Lio and Boulinguez, 2016).

Data-driven methods such as MCCA are attractive in that they find a mapping between subjects based only on shared temporal aspects of the data, without

596 requiring external information. MCCA and related methods have been widely  
 597 used for fMRI data (Li et al., 2009; Correa et al., 2010b; Hwang et al., 2012;  
 598 Afshin-Pour et al., 2012; Karhunen et al., 2013; Haxby et al., 2011; Afshin-Pour  
 599 et al., 2014) and EEG/MEG (Lankinen et al., 2014; Sturm, 2016; Zhang et al.,  
 600 2017). In contrast to MCCA, which finds variance dimensions that are similar  
 601 across subjects with no attempt to ensure that they correspond to sources within  
 602 the brain, ICA-based approaches attempt to to isolate sources common across  
 603 subjects based on criteria of statistical independence (Calhoun and Adali, 2012;  
 604 Eichele et al., 2011; Huster et al., 2015; Chen et al., 2016; Madsen et al.; Huster  
 605 and Raud, 2018). Group ICA (GICA) as formulated by Eichele et al. (2011) can  
 606 be seen as a concatenation of MCCA (as described here) with ICA. Isolating the  
 607 MCCA step, as we do here, is useful conceptually and avoids the computational  
 608 cost and assumptions associated with ICA. Hyperalignment, as used by Haxby et  
 609 al. (2011), is conceptually the same as MCCA but restricting the transformations  
 610 to rotations, i.e. Procrustes analysis (Xu et al., 2012). Hyperalignment has the  
 611 advantage to maintain metric distance of patterns in the original and transformed  
 612 space, but the disadvantage that it cannot favor channels with higher inter-subject  
 613 correlation.

614 The focus here is on *temporal patterns* common to all subjects and thus in the  
 615 MCCA procedure the data are concatenated along the spatial dimension (chan-  
 616 nels). It is also possible to extract *spatial patterns* common across subjects by  
 617 concatenating data along the temporal dimension. Methods for group analysis of  
 618 data from multiple subjects are reviewed by Correa et al. (2010a,b); Calhoun and  
 619 Adali (2012); Sui et al. (2012); Afshin-Pour et al. (2014); Dähne et al. (2015);  
 620 Chen et al. (2016); Huster and Raud (2018).

621 **Denoising and dimensionality reduction.** As described in the Methods and il-  
 622 lustrated in the Results, data from single subjects can be denoised by projecting on  
 623 the overcomplete basis of  $D$  CCs, truncating, and projecting back. Data dimen-  
 624 sions that are not shared with other subjects are *downweighted* but not removed,  
 625 so in general the rank of the data remains the same. Setting the cutoff  $\hat{D} < D$  to  
 626 a relatively high order suppresses only those components that are very different  
 627 from those found in other subjects, most likely to be noise. In Example 5, the set  
 628 of 40 PCs that represented each subject were transformed into 320 CCs, of which  
 629 110 were selected before being projected back to obtain “denoised” data, yielding  
 630 the benefit shown in Fig. 9. The CCs that were rejected absorbed some of the  
 631 subject-specific patterns of noise, improving the outcome.

632 It is often useful to reduce the dimensionality of the data for computational  
 633 reasons (to reduce memory or computation time), or to avoid overfitting. The  
 634 standard procedure of applying PCA and truncating the series of PCs implicitly  
 635 equates variance to relevance, which may not be justified, as artifact sources may  
 636 have high variance, and useful sources may be weak. MCCA is of use in this  
 637 respect to replace the variance criterion by a criterion of consistency with other  
 638 data. This can be done conservatively by removing a small fraction of SCs that  
 639 represent the most atypical patterns within the data set.

640 As a tool to analyze or denoise the data of a single subject, MCCA is compa-  
 641 rable to data-driven linear analysis techniques such as PCA, Independent Compo-  
 642 nent Analysis (ICA), Joint Diagonalization, CCA and others. The fact that it uses  
 643 a different criterion makes it *complementary* to those methods as a denoising or  
 644 dimensionality reduction tool (e.g one can apply MCCA before or after ICA, JD,  
 645 etc.).

646 **Caveats and cautions.** A risk, common to other data-driven methods such as  
 647 ICA or JD, is circularity of the analysis (Kriegeskorte et al., 2009). The method  
 648 is designed to optimize correlation between data matrices, and therefore the ob-  
 649 servation that the components that it finds *are* correlated between data matrices  
 650 is of little weight, unless corroborated by careful cross-validation. Related to this  
 651 issue is overfitting: each SC depends on  $D = \sum_n d_n$  parameters, a number that  
 652 can be large if there are many data matrices involved. Overfitting can be detected  
 653 using resampling and cross-validation methods, and the risk of overfitting can be  
 654 reduced by dimensionality reduction or other regularization techniques.

655 MCCA can easily latch on to artefacts and noise patterns shared across data  
 656 matrices. Uninteresting linear or polynomial trends (for example EEG drift po-  
 657 tentials) may thus appear among the first MCCA components. More generally,  
 658 MCCA can be biased towards narrowband or low-frequency components com-  
 659 mon across data matrices, *even if their phase is not aligned*, particularly if the  
 660 noise is spectrally-shaped or contains narrow-band components. This is illus-  
 661 trated in Fig. 12 that shows the result of applying MCCA to ten “data matrices”,  
 662 each of 12 s duration, extracted at random from the same 40-channel EEG data  
 663 that was used as background noise in Example 3. No known signal is common  
 664 across these data matrices, nonetheless the lowest-order SCs have narrow spectra  
 665 (Fig. 12 left) and quasi-sinusoidal waveforms (right) that might make them seem  
 666 significant. It is easy to understand why MCCA might take such components to  
 667 be shared: a sinusoid of arbitrary phase can be expressed as the weighted sum of  
 668 a sine and a cosine, and thus narrowband activity can be approximated as result-  
 669 ing from two sinusoidal components in quadrature phase. As this is the case for  
 670 all datasets, MCCA will select the two-component sinusoidal basis as common.  
 671 Such spurious components compete with genuine shared activity, complicating  
 672 the analysis.

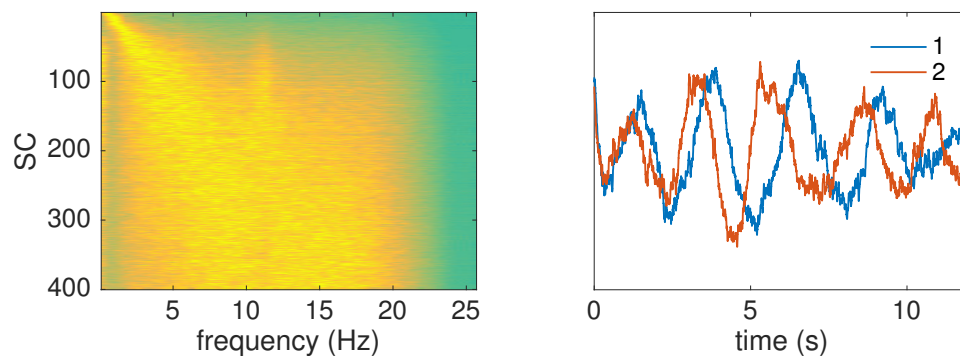


*Figure 12: MCCA's bias towards narrowband and low-frequency activity. Left: power spectra of SCs derived from an MCCA analysis of 10 EEG “data matrices” of duration 12 s randomly sampled from 40-channel EEG data. Power is coded as color. Right: time course of the first two SCs.*

673 MCCA assumes that temporal patterns are common across data matrices. A  
674 difference in latency of a brain response between different subjects may reduce the  
675 ability of MCCA to extract this activity. A common outcome in that case is two  
676 components, one with a shape similar to the average pattern over subjects, and the  
677 other similar to their difference (or derivative). MCCA can readily be extended to  
678 include time-lags to account for differences in response latency between subjects,  
679 although this comes at the expense of a greater number of parameters and a greater  
680 risk of overfitting. MCCA is obviously of no benefit in the absence of synchronous  
681 patterns, for example it is not well suited for analyzing resting-state data of a group  
682 of subjects.

683 MCCA yields both CCs and SCs, either of which can be exploited. When  
684 reporting, it is important to specify which, to avoid confusion. As an example, the  
685 phrase ‘MCCA was applied as a preprocessing step’ is not sufficient to specify  
686 what was done.

687 **Applicability to real-time processing.** This work was motivated in part by the  
688 need to steer an auditory assistive device using brain signals. An obstacle to reli-

able decoding is the high-level of noise and artifacts in the EEG signals, and analysis and denoising methods are essential for the success of this application. To be useful, a method must be applicable to *real-time* processing, whereas MCCA as described here works in batch mode. It may nonetheless be of use in the following fashion. EEG data is recorded from a pool of subjects to a calibration sample of speech, and MCCA is used to derive a “canonical” EEG response to that sample. To adapt the system to a new user, EEG data are recorded in response to the calibration sample, and a spatial filter is designed (for example using CCA) to maximize similarity between the subject’s and the canonical response. This spatial filter is then used in the real-time processing pipeline. This suggests that MCCA can also be put to use in a practical application such as cognitive control of a hearing aid.

## 5 Conclusion

Multiway CCA is a powerful tool for analysis of multi-subject multivariate datasets. It can be used both to design spatial filters to denoise data of each individual subject, and to summarize data across subjects. Many related methods have been proposed in the literature, but the processing principles behind them, and the range of tasks that they can be used for, are not widely appreciated. The use of MCCA (or similar techniques) should be more prevalent given the ubiquitous need for merging data across subjects. In this paper we presented a formulation of MCCA that is relatively easy to understand, illustrated in detail how it works, and showed how it can be put to use for a wide range of common tasks in multi-subject multivariate data analysis.

## 712 Acknowledgements

713 This work was supported by the EU H2020-ICT grant 644732 (COCOHA), and  
 714 grants ANR-10-LABX-0087 IEC and ANR-10-IDEX-0001-02 PSL\*. Lucas C.  
 715 Parra received support from the National Science Foundation under grant DRL-  
 716 1660548. Some of these ideas were tried out at the 2017 Telluride Neuromorphic  
 717 Engineering Workshop. Malcolm Slaney and Sam Norman-Haignière offered use-  
 718 ful comments on earlier versions of the manuscript.

## 719 References

- 720 Afshin-Pour B, Grady C, Strother S (2014) Evaluation of spatio-temporal decom-  
 721 position techniques for group analysis of fMRI resting state data sets. *NeuroIm-*  
 722 *age* 87:363–382.
- 723 Afshin-Pour B, Hossein-Zadeh GA, Strother SC, Soltanian-Zadeh H (2012) En-  
 724 hancing reproducibility of fMRI statistical maps using generalized canonical  
 725 correlation analysis in NPAIRS framework. *NeuroImage* 60:1970–1981.
- 726 Asendorf NA (2015) Informative Data Fusion : Beyond Canonical Correlation  
 727 Analysis Ph.D. diss., University of Michigan.
- 728 Benton A, Khayrallah H, Gujral B, Reisinger DA, Zhang S, Arora R (2017) Deep  
 729 Generalized Canonical Correlation Analysis. *ArXiv* arXiv:1702.
- 730 Calhoun VD, Adali T (2012) Multisubject independent component analysis of  
 731 fMRI: A decade of intrinsic networks, default mode, and neurodiagnostic dis-  
 732 covery. *IEEE Reviews in Biomedical Engineering* 5:60–73.
- 733 Chait M, de Cheveigné A, Poeppel D, Simon JZ (2010) Neural dynam-



- 734 ics of attending and ignoring in human auditory cortex. *Neuropsycholo-*  
735 *gia* 48:3262–3271.
- 736 Chen X, Wang ZJ, McKeown M (2016) Joint Blind Source Separation for Neuro-  
737 physiological Data Analysis: Multiset and multimodal methods. *IEEE Signal*  
738 *Processing Magazine* 33:86–107.
- 739 Choi I, Rajaram S, Varghese LA, Shinn-Cunningham BG (2013) Quantifying  
740 attentional modulation of auditory-evoked cortical responses from single-trial  
741 electroencephalography. *Frontiers in Human Neuroscience* 7.
- 742 Correa NM, Adalı T, Li YO, Calhoun VD (2010a) Canonical correlation anal-  
743 ysis for data fusion and group inferences. *IEEE Signal Processing Maga-*  
744 *zine* July:39–50.
- 745 Correa NM, Eichele T, Adalı T, Li YO, Calhoun VD (2010b) Multi-set canonical  
746 correlation analysis for the fusion of concurrent single trial ERP and functional  
747 MRI. *Neuroimage* 50:1438–1445.
- 748 Crosse MJ, Di Liberto GM, Bednar A, Lalor EC (2016) The Multivariate Tem-  
749 poral Response Function (mTRF) Toolbox: A MATLAB Toolbox for Re-  
750 lating Neural Signals to Continuous Stimuli. *Frontiers in Human Neuro-*  
751 *science* 10:1–14.
- 752 Cunningham JP, Yu BM (2014) Dimensionality reduction for large-scale neural  
753 recordings. *Nature Neuroscience* 17:1500–1509.
- 754 Dähne S, Bießman F, Samek W, Haufe S, Goltz D, Gundlach C, Villringer A, Fazli  
755 S, Müller KR (2015) Multivariate Machine Learning Methods for Fusing Func-  
756 tional Multimodal Neuroimaging Data. *Proceedings of the IEEE* 103:1–22.

- 757 de Cheveigné A, Arzounian D (2018) Robust detrending, rereferencing, outlier  
758 detection, and inpainting of multichannel data. *NeuroImage* 172:903–912.
- 759 de Cheveigné A, Parra LC (2014) Joint decorrelation, a versatile tool for multi-  
760 channel data analysis. *NeuroImage* 98:487–505.
- 761 de Cheveigné A, Simon JZ (2008) Denoising based on spatial filtering. *Journal*  
762 *of neuroscience methods* 171:331–339.
- 763 de Cheveigné A, Wong D, Liberto GMD, Hjortkjaer J, Slaney M, Lalor E (2018)  
764 Decoding the auditory brain with canonical correlation analysis. *NeuroIm-*  
765 *age* 172:206–216.
- 766 Di Liberto GM, O’Sullivan JA, Lalor EC (2015) Low-Frequency Cortical En-  
767 trainment to Speech Reflects Phoneme-Level Processing. *Current biology : CB*  
768 25:2457–2465.
- 769 Ding N, Simon JZ (2012) Neural coding of continuous speech in auditory cortex  
770 during monaural and dichotic listening. *Journal of Neurophysiology* 107:78–89.
- 771 Dmochowski JP, Ki JJ, DeGuzman P, Sajda P, Parra LC (2017) Extracting multi-  
772 dimensional stimulus-response correlations using hybrid encoding-decoding of  
773 neural activity. *NeuroImage* pp. 1–13.
- 774 Dmochowski JP, Sajda P, Dias J, Parra LC (2012) Correlated Components of  
775 Ongoing EEG Point to Emotionally Laden Attention A Possible Marker of En-  
776 gagement? *Frontiers in Human Neuroscience* 6:112.
- 777 Eichele T, Rachakonda S, Brakedal B, Eikeland R, Calhoun VD (2011) EEGIFT:  
778 Group independent component analysis for event-related EEG data. *Computa-*  
779 *tional Intelligence and Neuroscience* 2011.

- 780 Fu X, Huang K, Hong M, Sidiropoulos ND, So AMC (2017) Scalable and Flexible  
781 Multiview MAX-VAR Canonical Correlation Analysis. *IEEE Transactions on*  
782 *Signal Processing* 65:4150–4165.
- 783 Fuglsang SA, Dau T, Hjortkjær J (2017) Noise-robust cortical tracking of attended  
784 speech in real-world acoustic scenes. *NeuroImage* 156:435–444.
- 785 Gross SM, Tibshirani R (2015) Collaborative regression. *Biostatistics*  
786 16:326–338.
- 787 Hasson U, Nir Y, Levy I, Fuhrmann G, Malach R (2004) Natural Vision. *Science*  
788 303:1634–1640.
- 789 Haufe S, Meinecke F, Görgen K, Dähne S, Haynes JD, Blankertz B, Bießmann F  
790 (2014) On the interpretation of weight vectors of linear models in multivariate  
791 neuroimaging. *NeuroImage* 87:96–110.
- 792 Haxby JV, Guntupalli JS, Connolly AC, Halchenko YO, Conroy BR, Gobbini MI,  
793 Hanke M, Ramadge PJ (2011) A common, high-dimensional model of the  
794 representational space in human ventral temporal cortex. *Neuron* 72:404–416.
- 795 Holdgraf CR, Rieger JW, Micheli C, Martin S, Knight RT, Theunissen FE (2017)  
796 Encoding and Decoding Models in Cognitive Electrophysiology. *Frontiers in*  
797 *Systems Neuroscience* 11.
- 798 Hotelling H (1936) Relations Between Two Sets of Variates.  
799 *Biometrika* 28:321–377.
- 800 Huster RJ, Plis SM, Calhoun VD (2015) Group-level component analyses of  
801 EEG: validation and evaluation. *Frontiers in Neuroscience* 9:1–14.
- 802 Huster RJ, Raud L (2018) A Tutorial Review on Multi-subject Decomposition of  
803 EEG. *Brain Topography* 31:1–14.

- 804 Hwang H, Jung K, Takane Y, Woodward TS (2012) Functional Multiple-Set  
805 Canonical Correlation Analysis. *Psychometrika* 77:48–64.
- 806 Karhunen J, Hao T, Ylipaavalniemi J (2013) Finding dependent and independent  
807 components from related data sets: A generalized canonical correlation analysis  
808 based method. *Neurocomputing* 113:153–167.
- 809 Kettenring J (1971) Canonical analysis of several sets of variables.  
810 *Biometrika* 58:433–451.
- 811 Khalighinejad B, Cruzatto da Silva G, Mesgarani N (2017) Dynamic Encoding  
812 of Acoustic Features in Neural Responses to Continuous Speech. *Journal of*  
813 *Neuroscience* 37:2176–2185.
- 814 Kiers HAL, Cl  roux R, Ten Berge JMF (1994) Generalized canonical analysis  
815 based on optimizing matrix correlations and a relation with IDIOSCAL. *Com-*  
816 *putational Statistics and Data Analysis* 18:331–340.
- 817 Koskinen M, Sepp   M (2014) Uncovering cortical MEG responses to listened  
818 audiobook stories. *NeuroImage* 100:263–270.
- 819 Kriegeskorte N, Simmons WK, Bellgowan PSF, Baker CI (2009) Circular anal-  
820 ysis in systems neuroscience: the dangers of double dipping. *Nature Neuro-*  
821 *science* 12:535–540.
- 822 Lalor EC, Power AJ, Reilly RB, Foxe JJ (2009) Resolving Precise Temporal Pro-  
823 cessing Properties of the Auditory System Using Continuous Stimuli. *Journal*  
824 *of Neurophysiology* 102:349–359.
- 825 Lankinen K, Saari J, Hari R, Koskinen M (2014) Intersubject consistency of  
826 cortical MEG signals during movie viewing. *NeuroImage* 92:217–224.

- 827 Lankinen K, Saari J, Hlushchuk Y, Tikka P, Parkkonen L, Hari R, Koskinen M  
828 (2018) Consistency and similarity of meg-and fmri-signal time courses during  
829 movie viewing. *NeuroImage* 173:361–369.
- 830 Li YO, Adali T, Wang W, Calhoun VD (2009) Joint blind source separation by  
831 multiset canonical correlation analysis. *IEEE Transactions on Signal Process-*  
832 *ing* 57:3918–3929.
- 833 Lio G, Boulinguez P (2016) How Does Sensor-Space Group Blind Source Sepa-  
834 ration Face Inter-individual Neuroanatomical Variability? Insights from a Sim-  
835 ulation Study Based on the PALS-B12 Atlas. *Brain Topography* 31:1–14.
- 836 Litvak V, Friston K (2008) Electromagnetic source reconstruction for group stud-  
837 ies. *NeuroImage* 42:1490–1498.
- 838 Luck SJ (2005) *An Introduction to the Event-Related Potential Technique* The  
839 MIT Press.
- 840 Madsen KH, Churchill NW, Mørup M Quantifying functional connectivity  
841 in multi?subject fmri data using component models. *Human Brain Map-*  
842 *ping* 38:882–899.
- 843 Mahjoory K, Nikulin VV, Botrel L, Linkenkaer-Hansen K, Fato MM, Haufe S  
844 (2017) Consistency of EEG source localization and connectivity estimates.  
845 *NeuroImage* 152:590–601.
- 846 Martin S, Brunner P, Holdgraf C, Heinze HJ, Crone NE, Rieger J, Schalk G,  
847 Knight RT, Pasley BN (2014) Decoding spectrotemporal features of overt and  
848 covert speech from the human cortex. *Frontiers in neuroengineering* 7:14.
- 849 Melzer T, Reiter M, Bischof H (2001) Nonlinear Feature Extraction Using Gener-  
850 alized Canonical Correlation Analysis. *ICANN 2001, LNCS 2130* pp. 353–360.

- 851 Mesgarani N, Chang EF (2012) Selective cortical representation of attended  
852 speaker in multi-talker speech perception. *Nature* 485:233–6.
- 853 Mirkovic B, Debener S, Jaeger M, Vos MD (2015) Decoding the attended speech  
854 stream with multi-channel EEG: implications for online, daily-life applications.  
855 *Journal of Neural Engineering* 12:046007.
- 856 Norman-Haignere S, Kanwisher NG, McDermott JH (2015) Distinct Cortical  
857 Pathways for Music and Speech Revealed by Hypothesis-Free Voxel Decom-  
858 position. *Neuron* 88:1281–1296.
- 859 O’Sullivan JA, Power AJ, Mesgarani N, Rajaram S, Foxe JJ, Shinn-Cunningham  
860 BG, Slaney M, Shamma SA, Lalor EC (2014) Attentional Selection in a Cock-  
861 tail Party Environment Can Be Decoded from Single-Trial EEG. *Cerebral Cor-  
862 tex* 25:1697–1706.
- 863 Parra L (2018) Multi-set canonical correlation analysis simply explained.  
864 *arXiv* arXiv:1802.03759.
- 865 Parra L, Haufe S, Dmochowski J (2018) Correlated components analysis - ex-  
866 tracting reliable dimensions in multivariate data. *arXiv* arXiv:1801.08881v2.
- 867 Southwell R, Baumann A, Gal C, Barascud N, Friston K, Chait M (2017)  
868 Is predictability salient? A study of attentional capture by auditory pat-  
869 terns. *Philosophical Transactions of the Royal Society B: Biological Sci-  
870 ences* 372:20160105.
- 871 Sturm I (2016) Analyzing the Perception of Natural Music with EEG and ECoG  
872 Ph.D. diss., Technischen Universität Berlin.
- 873 Sui J, Adali T, Yu Q, Chen J, Calhoun VD (2012) A review of multivariate

- 874 methods for multimodal fusion of brain imaging data. *Journal of Neuroscience*  
875 *Methods* 204:68–81.
- 876 Takane Y, Hwang H, Abdi H (2008) Regularized multiple-set canonical correla-  
877 tion analysis. *Psychometrika* 73:753–775.
- 878 Tenenhaus A (2011) Regularized Generalized Canonical Correlation Analysis and  
879 PLS Path Modeling. *Psychometrika* 76:257–284.
- 880 Tenenhaus A, Philippe C, Frouin V (2015) Kernel Generalized Canonical Corre-  
881 lation Analysis. *Computational Statistics and Data Analysis* 90:114–131.
- 882 Tiitinen H, Miettinen I, Alku P, May PJC (2012) Transient and sustained cortical  
883 activity elicited by connected speech of varying intelligibility. *BMC Neuro-*  
884 *science* 13:157.
- 885 van de Velden M, Takane Y (2012) Generalized canonical correlation analysis  
886 with missing values. *Computational Statistics* 27:551–571.
- 887 Velden MVD (2011) On generalized canonical correlation analysis. *Proc. 58th*  
888 *World Statistical Conference* pp. 758–765.
- 889 Via, Javier, Ignacio Santamaria, Pérez J (2005) Canonical correlation analysis  
890 (CCA) algorithms for multiple data sets: Application to blind SIMO equaliza-  
891 tion. *Signal Processing Conference* 1:4–7.
- 892 Witten DM, Tibshirani RJ (2009) Extensions of Sparse Canonical Correlation  
893 Analysis with Applications to Genomic Data. *Statistical Applications in Ge-*  
894 *netics and Molecular Biology* 8:29.
- 895 Xu H, Lorbert A, Ramadge PJ, Guntupalli JS, Haxby JV (2012) Regularized hy-  
896 peralignment of multi-set fmri data In *Statistical Signal Processing Workshop*  
897 *(SSP), 2012 IEEE*, pp. 229–232. IEEE.

- 898 Zhang Q, Borst JP, Kass RE, Anderson JR (2017) Inter-subject alignment  
899 of MEG datasets in a common representational space. *Human Brain Map-*  
900 *ping* 38:4287–4301.
- 901 Zhang Y, Zhou G, Zhao Q, Onishi A, Jin J, Wang X, Cichocki A (2011) Multiway  
902 canonical correlation analysis for frequency components recognition in ssvep-  
903 based bcis pp. 287–295.
- 904 Zion Golumbic EM, Ding N, Bickel S, Lakatos P, Schevon CA, McKhann GM,  
905 Goodman RR, Emerson R, Mehta AD, Simon JZ, Poeppel D, Schroeder CE  
906 (2013) Mechanisms underlying selective neuronal tracking of attended speech  
907 at a "cocktail party". *Neuron* 77:980–991.